Inorg. Chem. **2006**, *45*, 1305–1315

Chemistry and Electrochemistry of the Heterodinuclear Complex ClPd(dppm)$_2$PtCl: A M–M′ Bond Providing Site Selectivity

David Evrard,[†,‡] Sébastien Clément,[§] Dominique Lucas,[†] Bernard Hanquet,[†] Michael Knorr,*[,§] Carsten Strohmann,[||] Andreas Decken,[⊥] Yves Mugnier,*[,†] and Pierre D. Harvey*[,‡]

Laboratoire de Synthèse et d'Electrosynthèse Organométalliques (LSEO−CNRS UMR 5188), Faculté des Sciences Mirande, Université de Bourgogne, 9 Allée A. Savary, 21000 Dijon, France, Département de Chimie, Université de Sherbrooke, Sherbrooke, J1K 2R1 Québec, Canada, Laboratoire de Chimie des Matériaux et Interfaces, Faculté des Sciences et des Techniques, Université de Franche-Comté, 16 route de Gray, 25030 Besançon, France, Institut für Anorganische Chemie, Universität Würzburg, Am Hubland, D-97074 Würzburg, Germany, and Department of Chemistry, University of New Brunswick, Fredericton, E3B 6E2 New Brunswick, Canada

Received July 1, 2005

The heterodinuclear d^9–d^9 title compound **1**, whose crystal structure has been solved, reacts with dppm [bis(diphenylphosphino)methane] in the presence of $NaBF_4$ to generate the salt [ClPd(μ-dppm)$_2$Pt(η^1-dppm)][BF_4] (**2a**), which contains a Pt-bound dangling dppm ligand. **2a** has been characterized by ^{1}H and ^{31}P NMR, Fourier transform Raman [ν(Pd–Pt) = 138 cm^{-1}], and UV–vis spectroscopy [λ_{max}(dσ–dσ*) = 366 nm]. In a similar manner, [ClPd(μ-dppm)$_2$Pt(η^1-dppm═O)][BF_4] (**2b**), ligated with a dangling phosphine oxide, has been prepared by the addition of dppm═O. The molecular structure of **2b** has been established by an X-ray diffraction study. **2a** reacts with 1 equiv of $NaBH_4$ to form the platinum hydride complex [(η^1-dppm)Pd(μ-dppm)$_2$Pt(H)][BF_4] (**3**). Both **2a** and **3** react with an excess of $NaBH_4$ to provide the mixed-metal d^{10}–d^{10} compound [Pd(μ-dppm)$_3$Pt] (**4**). The photophysical properties of **4** were studied by UV–vis spectroscopy [λ_{max}(dσ–dσ*) = 460 nm] and luminescence spectroscopy (λ_{emi} = 724 nm; $\tau_e = 12 \pm 1$ μs, 77 K). The protonation of **1** and **4** leads to [ClPd(μ-dppm)$_2$(μ-H)PtCl]$^+$ (**5**) and **3**, respectively. Stoichiometric treatment of **1** with cyclohexyl or xylyl isocyanide yields [ClPd(μ-dppm)$_2$Pt(CNC_6H_{11})]Cl (**6a**) and [ClPd(μ-dppm)$_2$Pt(CN–xylyl)]Cl (**6b**) ligated by terminal-bound CNR ligands. In contrast, treatment of **1** with the phosphonium salt [C≡NCH_2PPh_3]Cl affords the structurally characterized A-frame compound [ClPd(μ-dppm)$_2$(μ-C═NCH_2PPh_3)PtCl]Cl (**6c**), spanned by a bridging isocyanide ligand. The electrochemical reduction of **2a** at –1.2 V vs SCE, as well as the reduction of **5** in the presence of dppm, leads to a mixture of products **3** and **4**. Further reduction of **3** at –1.7 V vs SCE generates **4** quantitatively. The reoxidation at 0 V of **4** in the presence of Cl^- ions produces back complex **2a**. The whole mechanism of the reduction of **1** has been established.

Introduction

Heterometallic complexes, in which the adjacent metal centers are linked by metal−metal bonds, represent interesting systems for the coordination and activation of small molecules. The polarity of the M−M′ bond, site selectivity for ligand substitution, and cooperative effects for substrate activation, as well as relevance to homogeneous and heterogeneous catalysis, have been dealt with in various reviews and monographs.[1−5] Even heterometallic systems incorporat-

* To whom correspondence should be addressed. E-mail: michael.knorr@univ-fcomte.fr (M.K.), yves.mugnier@u-bourgogne.fr (Y.M.), pharvey@usherbrooke.ca (P.D.H.). Tel: (819) 821-7092 (P.D.H.), (33) 3 80 39 60 91 (Y.M.). Fax: (819) 821-8017 (P.D.H.), (33) 3 80 39 60 91 (Y.M.).
[†] Université de Bourgogne.
[‡] Université de Sherbrooke.
[§] Université de Franche-Comté.
[||] Universität Würzburg.
[⊥] University of New Brunswick.

(1) Adams, D. A., Cotton, F. A., Eds. *Catalysis by Di- and Polynuclear Metal Cluster Complexes*; Wiley-VCH: New York, 1998.
(2) Braunstein, P., Oro, L. A., Raithby, P. R, Eds. *Metal Clusters in Chemistry*; Wiley-VCH: Weinheim, Germany, 1999.
(3) Wheatley, N.; Kalck, P. *Chem. Rev.* **1999**, *99*, 3379.
(4) (a) Chaudret, B.; Delavaux, B.; Poilblanc, R. *Coord. Chem. Rev.* **1988**, *86*, 191. (b) Mague, J. T. *J. Cluster Sci.* **1995**, *6*, 217.
(5) (a) Tsuji, J. *Palladium Reagents and Catalysts*; Wiley: New York, 1995. (b) Moiseev, I.; Vargaftik, M. N. *New J. Chem.* **1998**, 1217.

10.1021/ic051102z CCC: $33.50
Published on Web 01/10/2006

ing metal centers from the same triad may show different reactivities as compared to their homometallic counterparts. Protonation of the complexes $[Cp(OC)_2M(\mu\text{-}PPh_2)Pt(CO)(PPh_3)]$ (M = Mo, W) exhibits an M-dependent site selectivity, with protonation occurring at the metal−metal bond for Mo to give $[Cp(OC)_2Mo(\mu\text{-}PPh_2)(\mu\text{-}H)Pt(CO)(PPh_3)]^+$, while in the case of tungsten, the terminal hydride cation $[Cp(OC)_2(H)W(\mu\text{-}PPh_2)(Pt(CO)(PPh_3)]^+$ is obtained.[6a] As demonstrated by Knox et al., the chemistry of the asymmetric system $[Cp(OC)_2Fe(\mu\text{-}CO)_2RuCp(CO)_2]$ does not fall between those of its symmetric Fe−Fe and Ru−Ru counterparts and exhibits enhanced reactivity toward alkynes.[6b] Another recent example concerns alkyne activation by the trinuclear chain complex $[Pt_2Pd(\mu\text{-dpmp})_2(CNR)_2](PF_6)$ (dpmp = {[bis(diphenylphosphino)methyl]phenyl}phosphine), in which the presence of Pd alters the reactivity compared to that of the analogous Pt−Pt−Pt chain complex.[6c]

A somewhat related system is the heterodinuclear M_2-bonded d^9−d^9 compound $[ClPd(\mu\text{-dppm})_2PtCl]$ (**1**), which was first reported by Pringle and Shaw 20 years ago.[7] The reactivity of this compound has been studied by several groups and can be divided roughly into three patterns: (i) insertion of small molecules such as SO_2, CS_2, and CO into the metal−metal bond gives rise to A-frame compounds; (ii) substitution of the axial chloro ligands by various anionic nucleophiles X^- affords the derivatives $[XPd(\mu\text{-dppm})_2PtX]$ [X = I, Br, SCN, alkyl, $NCMnCp(CO)_2$];[8] (iii) furthermore, the complex has become a good starting material for the construction of heterotri- and tetranuclear clusters via the initial attack of metalates L_nM^- on the M−Cl bond and subsequent migration of one of the Pd-bound dppm phosphorus atoms on M, forming a triangular Pd−Pt−M core.[9,10]

We now report the chemical and electrochemical reactivities of the title complex **1** toward the addition of dppm, dppm═O, isocyanide, H^- (from $NaBH_4$), and H^+. Our results demonstrate that, despite the close chemical behavior between Pd and Pt, this d^9−d^9 system exhibits a pronounced site selectivity toward electrophilic and nucleophilic attack. Moreover, this is the first detailed electrochemical study on this interesting heterobimetallic compound; the electrochemical reduction of the various species in the presence of dppm has been investigated, and some molecular structures are presented.

Experimental Section

Materials. Compound **1**, dppm═O, and $[C{\equiv}NCH_2PPh_3]Cl$ were prepared according to a literature procedure.[7,11,12] The solvents were purified according to standard procedures.[13] All manipulations were performed using Schlenk techniques in an atmosphere of dry oxygen-free argon.

$[ClPd(\mu\text{-dppm})_2Pt(\eta^1\text{-dppm})][BF_4]$ (2a). In a 250-mL flask, 114 mg (0.1 mmol) of **1** was suspended in 50 mL of tetrahydrofuran (THF). A total of 50 mg (0.13 mmol) of dppm and 44 mg (0.4 mmol) of $NaBF_4$ were added to this suspension. The mixture, which became gradually clear, was stirred for 1 day at 298 K, filtered, and evaporated to dryness. The orange solid was extracted with 10 mL of CH_2Cl_2. Layering of the extract with Et_2O afforded yellow crystals of **2a**, solvated with 0.5 molecule of CH_2Cl_2, in 71% yield (114 mg). Anal. Calcd for $C_{75}H_{66}BClF_4P_6PdPt{\cdot}0.5CH_2Cl_2$: C, 56.01; H, 4.17. Found: C, 56.24; H, 4.22. ^{1}H NMR (acetone-d_6): δ 8.72−6.64 (m, 60H, Ph), 5.55 (m, br, 2H, PCH_2P), 4.84 (m, 4H, PCH_2P, $^3J_{Pt-H}$ = 128.0 Hz). $^{31}P\{^1H\}$ NMR (acetone-d_6): 5.3 (m, Pt−$P(\eta^1$-dppm), $^1J_{Pt-P}$ = 2121 Hz), −1.7 (m, Pt−$P(\mu$-dppm), $^1J_{Pt-P}$ = 2930 Hz), −3.8 (m, Pd−$P(\mu$-dppm)), −26.7 (d, Pt−PCH_2P, $^2J_{P-P}$ = 54 Hz, $^3J_{Pt-P}$ = 19 Hz). FT Raman (solid): 138 cm^{-1} (ν(PdPt)). UV−vis (acetone): λ_{max} = 366 nm (ϵ = 6274 M^{-1} cm^{-1}).

$[ClPd(\mu\text{-dppm})_2Pt(\eta^1\text{-dppm═O})]BF_4$ (2b). To a suspension of **1** (114 mg, 0.1 mmol) in THF (50 mL) were added dppm═O (121 mg, 0.3 mmol) and 44 mg (0.4 mmol) of $NaBF_4$. The mixture, which became gradually clear, was stirred for 1 day at 298 K, filtered, and evaporated to dryness. The orange solid was extracted with 10 mL of CH_2Cl_2. Layering of the extract with Et_2O afforded orange crystals of **2b**, solvated with 1 molecule of CH_2Cl_2, in 66% yield (111 mg). Anal. Calcd for $C_{75}H_{66}BClF_4OP_6PdPt{\cdot}CH_2Cl_2$: C, 54.40; H, 4.09. Found: C, 54.46; H, 4.44. ^{1}H NMR ($CDCl_3$): 8.78−6.52 (m, 60H, Ph); 6.60 (m, 2H, PCH_2P), 4.25 (m, 4H, PCH_2P, $^3J_{Pt-H}$ = 120.0 Hz). $^{31}P\{^1H\}$ NMR ($CDCl_3$): 23.4 (d, Pt−PCH_2P═O, $^2J_{P-P}$ = 7 Hz), 4.0 (m, Pt−$P(\eta^1$-dppm)), $^1J_{Pt-P}$ = 2242 Hz), −3.9 (m, Pt−$P(\mu$-dppm), $^1J_{Pt-P}$ = 2944 Hz), −5.8 (m, Pd−$P(\mu$-dppm)). FABMS (rel intens): 1505.5 (6%) $PdPt(dppm)_3ClO$, 1489.9 (12%) $PdPt(dppm)_3O$, 1454.0 (9%) $PdPt(dppm)_3$, 1104.9 (100%) $PdPt(dppm)_2Cl$, 1070.0 (79%) $PdPt(dppm)_2$.

$[(\eta^1\text{-dppm})Pd(\mu\text{-dppm})_2Pt(H)][BF_4]$ (3). A total of 3 μL (0.080 mmol) of HCO_2H was added to a 50-mL THF solution containing 100 mg (0.069 mmol) of **4**. The solution was stirred for 1 h in the presence of $NaBF_4$ and evaporated to dryness. The orange residue was washed with 10 mL of Et_2O and dried in a vacuum. Alternatively, **3** has been prepared by direct addition of $HBF_4{\cdot}Et_2O$. Yield: 85% (91 mg). Anal. Calcd for $C_{75}H_{67}BF_4P_6PdPt$: C, 58.40; H, 4.39. Found: C, 58.64; H, 4.83. ^{1}H NMR ($CDCl_3$): δ 7.72−6.59 (m, 60H, Ph); 4.11−3.99 (three signals corresponding to PCH_2P), −6.45 (d, broadened, 1H, Pt−*H*, $^1J_{Pt-H}$ = 707 Hz, $^2J_{P-H}$ = 165.0 Hz). $^{31}P\{^1H\}$ NMR ($CDCl_3$): δ −1.79 (m, Pt−P(μ-dppm), $^1J_{Pt-P}$ = 2829 Hz), −3.50 (m, Pd−P(μ-dppm)), −28.41 (d, Pd−

(6) (a) Powell, J.; Sawyer, J. F.; Smith, S. S. *J. Chem. Soc., Chem. Commun.* **1985**, 1312. (b) Dennett, J. N. L.; Knox, S. A. R.; Anderson, K. M.; Charmant, J. P. H.; Orpen, A. G. *J. Chem. Soc., Dalton Trans.* **2005**, 63 and references cited therein. (c) Tanase, T.; Begum, R. A. *Organometallics* **2001**, *20*, 106.

(7) (a) Pringle, P. G.; Shaw, B. L. *J. Chem. Soc., Chem. Commun.* **1982**, 81. (b) Pringle, P. G.; Shaw, B. L. *J. Chem. Soc., Dalton Trans.* **1983**, 889.

(8) Braunstein, P.; Oswald, B.; Tiripicchio, A.; Ugozzoli, F. *J. Chem. Soc., Dalton Trans.* **2000**, 2195.

(9) (a) Braunstein, P.; Ries, M.; de Méric de Bellefon, C.; Dusausoy, Y.; Mangeot, J. P. *J. Organomet. Chem.* **1988**, *355*, 533. (b) Braunstein, P.; Oswald, B. *J. Organomet. Chem.* **1987**, *328*, 229. (c) Braunstein, P.; de Méric de Bellefon, C.; Ries, M. *Inorg. Chem.* **1988**, *27*, 1338. (d) Braunstein, P.; de Méric de Bellefon, C.; Ries, M.; Fischer, J. *Organometallics* **1988**, *7*, 332. (e) Braunstein, P.; Kervennal, J.; Richert, J. L. *Angew. Chem.* **1985**, *97*, 762. (f) Braunstein, P.; de Méric de Bellefon, C.; Ries, M. *J. Organomet. Chem.* **1984**, *262*, C14. (g) Braunstein, P.; de Méric de Bellefon, C.; Dusausoy, Y.; Bayeul, D. *J. Cluster Sci.* **1995**, *1*, 175. (h) Grossel, M. C.; Moulding, R. P.; Seddon, K. R. *J. Organomet. Chem.* **1983**, *253*, C50.

(10) Stockland, R. A., Jr.; Anderson, G. K.; Rath, N. P. *Inorg. Chim. Acta* **2000**, *300*−*302*, 395.

(11) Grushin, V. V. *Chem. Rev.* **2004**, *104*, 1629 and references cited therein.

(12) Zinner, G.; Fehlhammer, W. P. *Angew. Chem., Int. Ed., Engl.* **1985**, *24*, 979.

(13) (a) Perrin, D. D.; Armarego, W. L. F.; Perrin, D. R. *Purifications of laboratory chemicals*; Pergamon Press: Oxford, U.K., 1966. (b) Gordon, A. J.; Ford, R. A. *The chemist's companion, a handbook of practical data, techniques and references*; Wiley: New York, 1972; p 436.

PCH_2P, $^2J_{P-P}$ = 68 Hz). UV−vis (THF): λ_{max} = 428 nm (ϵ = 7308 M^{-1} cm^{-1}). IR (golden bridge): 1954 cm^{-1} (ν(Pt−H)).

[Pd(μ-dppm)$_3$Pt] (4). A total of 154 mg (0.40 mmol) of dppm was added to a THF solution (50 mL) containing 220 mg (0.20 mmol) of **1**. Then 1 mL of methanol containing 10 equiv of $NaBH_4$ (50 mg) was added. The solution, which turned to dark red, was stirred for 1 h and then evaporated to dryness. The orange-red residue was extracted with toluene (8 mL) and layered with Et_2O. After the residue was kept in a refrigerator for 2 days, orange-red crystals of **4** were formed. Yield: 59% (113 mg). No satisfactory elemental analysis could be obtained because of the presence of small amounts (ca. 5%) of [Pd(μ-dppm)$_3$Pd], which could not be removed by recrystallization. ^{1}H NMR (C_6D_6): δ 7.66−7.00 (m, 60H, Ph), 3.46 (m, 6H, PCH_2P, $^3J_{Pt-H}$ = 34.0 Hz). ^{31}P{^{1}H} NMR (C_6D_6): δ 11.9 (m, Pd−P), 42.9 (m, Pt−P, $^1J_{Pt-P}$ = 4430 Hz). FABMS (rel intens): 1453.0 (17%) PdPt(dppm)$_3$, 1070.0 (100%) PdPt(dppm)$_2$. UV−vis (THF): λ_{max} = 460 nm (ϵ = 10 159 M^{-1} cm^{-1}).

[ClPd(μ-dppm)$_2$Pt(H)Cl][BF$_4$] (5). A total of 17.5 μL (0.106 mmol) of HBF_4 (54 wt %) in diethyl ether was added to a 5-mL CH_2Cl_2 solution containing 100 mg (0.088 mmol) of **1**. The solution was stirred for 30 min and then evaporated to dryness. The yellow residue was rinsed with diethyl ether and dried. Yield: 90% (90 mg). Anal. Calcd for $C_{50}H_{45}BCl_2F_4P_4PdPt\cdot CH_2Cl_2$: C, 46.65; H, 3.61. Found: C, 46.62; H, 3.79. ^{1}H NMR ($CDCl_3$): δ 7.76−7.12 (m, 40 H, Ph), 4.48 (m, 4H, PCH_2P, $^3J_{Pt-H}$ = 53 Hz), −15.56 (qt, 1H, Pt-*H*, $^1J_{Pt-H}$ = 888 Hz, $^2J_{P-H}$ = 8 Hz). ^{31}P{^{1}H} NMR ($CDCl_3$): δ 13.6 (m, Pd−P, $^3J_{Pt-P}$ = 166 Hz), 11.1 (m, Pt−P, N = 77 Hz, $^1J_{Pt-P}$ = 2335 Hz). The PF_6 salt [ClPd(μ-dppm)$_2$Pt(H)Cl][PF_6] was prepared in a similar manner. LSIMS (rel intens): 1142.5 (16%) PdPt(dppm)$_2$Cl$_2$H, 1141.5 (18%) PdPt(dppm)$_2$Cl$_2$, 1105.8 (56%) PdPt(dppm)$_2$ClH, 1103.8 (100%) PdPt(dppm)$_2$Cl. UV−vis (THF): λ_{max} = 383 nm (ϵ = 10 030 M^{-1} cm^{-1}).

[ClPd(μ-dppm)$_2$Pt(CNC$_6$H$_{11}$)]Cl (6a). A solution of cyclohexyl isocyanide (12.5 μL, 0.1 mmol), diluted in 3 mL of CH_2Cl_2, was added within 30 min to a stirred solution of **1** (114 mg, 0.1 mmol) in 5 mL of CH_2Cl_2. The yellowish solution was concentrated, and yellow **6a** was precipitated by the addition of hexane. Yield: 72% (97 mg). Anal. Calcd For $C_{57}H_{55}Cl_2NP_4PdPt\cdot CH_2Cl_2$: C, 52.17; H, 4.30; N, 1.05. Found: C, 51.98; H, 4.12; N, 1.01. IR (CH_2Cl_2): 2197s cm^{-1} (ν(CN)). ^{31}P{^{1}H} NMR ($CDCl_3$): −6.1 (m, Pd−P, N = 86 Hz, $^{2+3}J_{Pt-P}$ = 78 Hz), −1.2 (m, Pt−P, $^1J_{Pt-P}$ = 2599 Hz).

[ClPd(μ-dppm)$_2$Pt(CN−xylyl)]Cl (6b). Xylyl isocyanide (13 mg, 0.1 mmol), diluted in 3 mL of CH_2Cl_2, was added within 30 min to a stirred solution of **1** (114 mg, 0.1 mmol) in 5 mL of CH_2Cl_2. The yellowish solution was reduced in volume and then layered with diethyl ether. After several days, yellow needles of **6b** were formed. Yield: 89% (120 mg). Anal. Calcd for $C_{59}H_{53}Cl_2NP_4PdPt\cdot CH_2Cl_2$: C, 53.01; H, 4.08; N, 1.03. Found: C, 53.48; H, 4.22; N, 1.22. IR (CH_2Cl_2): 2197s cm^{-1} (ν(CN)). ^{1}H NMR ($CDCl_3$): 2.11 (s, 6H, CH_3), δ 7.74−6.77 (m, 43H, Ph); 4.65 (m, br, 4H, PCH_2P, $^3J_{Pt-H}$ = 68.6 Hz). ^{31}P{^{1}H} NMR ($CDCl_3$): −6.2 (m, Pd−P, N = 88 Hz, $^{2+3}J_{Pt-P}$ = 126 Hz), −1.3 (m, Pt−P, $^1J_{Pt-P}$ = 2590 Hz). ^{195}Pt{^{1}H} NMR ($CDCl_3$): −2407 (tt, br, $^1J_{Pt-P}$ = 2590 Hz, $^{2+3}J_{Pt-P}$ = 126 Hz).

[ClPd(μ-dppm)$_2$(μ-C=NCH$_2$PPh$_3$)PtCl]Cl (6c). [C≡NCH_2PPh_3]Cl (34 mg, 0.1 mmol), diluted in 3 mL of CH_2Cl_2, was added within 30 min to a stirred solution of **1** (114 mg, 0.1 mmol) in 5 mL of CH_2Cl_2. The clear solution was reduced in volume and then layered with diethyl ether. Yellow crystals of **6c**, solvated with 1 molecule of CH_2Cl_2, were formed in 93% yield (146 mg). Anal. Calcd for $C_{70}H_{61}Cl_3NP_5PdPt\cdot CH_2Cl_2$: C, 54.53; H, 4.06; N, 0.90. Found: C, 54.87; H, 4.38; N, 0.95. IR (KBr): 1536w cm^{-1} (ν(C=N)). ^{31}P{^{1}H} NMR ($CDCl_3$): 15.9 (s, PPh_3CH_2), 14.9 (m, Pt−*P*, $^1J_{Pt-P}$ = 3383 Hz), 7.2 (m, Pd−*P*, $^3J_{Pt-P}$ = 423 Hz). ^{195}Pt{^{1}H} NMR ($CDCl_3$): −2306 (tt, $^1J_{Pt-P}$ = 3383 Hz, $^3J_{Pt-P}$ = 423 Hz).

Apparatus. The ^{31}P{^{1}H} NMR spectra were recorded on Bruker DRX 300 and DRX 500 spectrometers operating respectively at 300.13 and 500.13 MHz. The ^{195}Pt{^{1}H} NMR spectra were recorded on a Bruker Avance 300 machine (64.52 MHz for ^{195}Pt), the ^{195}Pt chemical shifts are externally referenced to K_2PtCl_4 in water, with downfield chemical shifts reported as positive. Fourier transform (FT) Raman spectra were acquired on a Bruker RFS 100/S spectrometer. IR spectra were recorded on a Bruker Vector 22 equipped with a golden-gate system. The UV−vis spectra were measured on a HP 8452A diode-array spectrophotometer. The emission lifetimes were measured with a nanosecond N_2 laser system from PTI model GL-3300 pumping a dye laser model GL-302. The pulse width is 2 ns, and the lower limit for the measurements was about 150−200 ps after deconvolution. The excitation wavelength was 400 nm. The continuous-wave emission spectra were measured on a SPEX Fluorolog II. Liquid secondary ion mass spectrometry (LSIMS) mass spectra were recorded on a Kratos CONCEPT 32S from the Centre de Spectroscopie Moléculaire of the Université de Bourgogne. The fast atom bombardment mass spectrometry (FABMS) data were acquired at the Université de Montréal, and the data analysis was simulated using a homemade program written in GW BASIC, computing all mathematically possible solutions for each fragment mass. Only the chemically meaningful solutions were retained using a window of ±2 g. All of the mass spectra were simulated in order to verify that for each peak the experimental isotope distribution pattern matches with the calculated one.

Electrochemical Experiments. The supporting electrolyte [Bu_4N][PF_6] was degassed under vacuum before use and then solubilized at a concentration of 0.2 M. For cyclic voltammetry (CV) experiments, the concentration of the analyte was nearly 10^{-3} M. Voltammetric analyses were carried out in a standard three-electrode cell with a Tacussel UAP4 unit cell. The reference electrode was a saturated calomel electrode (SCE) separated from the solution by a sintered-glass disk. The auxiliary electrode was a platinum wire. For all voltammetric measurements, the working electrode was a vitreous carbon electrode (ϕ = 3 mm). Under these conditions, during operation in THF, the formal potential for the ferrocene$^{+/0}$ couple is found to be +0.56 V vs SCE. The controlled potential electrolysis was performed with an Amel 552 potentiostat coupled with a Tacussel IG5-N integrator. A carbon gauze was used as the working electrode, a platinum plate as the counter electrode, and a SCE as the reference electrode.

Crystallography. Crystals of **1** were grown by layering using CH_2Cl_2/heptane at 20 °C. Single crystals were coated with Paratone-N oil, mounted using a glass fiber, and frozen in the cold nitrogen stream of the goniometer. A hemisphere of data was collected on a Bruker AXS P4/SMART 1000 diffractometer using ω and θ scans with a scan width of 0.3° and 10-s exposure times. The detector distance was 5 cm. The structure was solved by direct methods and refined by full-matrix least squares on F^2 (SHELXTL).[16] The metal atom positions were disordered over two sites and the occupancies determined using an isotropic model as 0.60 (Pt1 and Pd2) and 0.40 (Pt2 and Pd1) and fixed in subsequent

(14) *SAINT*, version 6.02; Bruker AXS Inc.: Madison, WI, 1997−1999.
(15) Sheldrick, G. *SADABS*; Bruker AXS Inc.: Madison, WI, 1999.
(16) *SHELXTL*, release 5.10; *The Complete Software Package for Single-Crystal Structure Determination*; Bruker AXS Inc.: Madison, WI, 1997.

Table 1. Crystal and Refinement Data for **1**, **2b**, and **6c**[a]

	1·$^1/_2CH_2Cl_2$	**2b**·CH_2Cl_2	**6c**·$3.25CH_2Cl_2$·C_4H_{10}
empirical formula	$C_{50.5}H_{45}Cl_3P_4PdPt$	$C_{76}H_{68}BCl_3F_4OP_6PdPt$	$C_{75.75}H_{72.50}Cl_{10.50}NP_5PdPt$
fw	1183.58	1677.77	1825.41
description	orange	orange	yellow
cryst size (mm)	0.075 × 0.4 × 0.4	0.175 × 0.275 × 0.3	0.30 × 0.20 × 0.20
temp (K)	198(1)	198(1)	173(2)
cryst syst	monoclinic	monoclinic	monoclinic
space group	*P*2(1)/*c*	*P*2(1)/*n*	*P*2(1)/*c*
a (Å)	13.5065(7)	13.4120(8)	22.008(3)
b (Å)	16.3073(8)	24.5549(15)	16.076(2)
c (Å)	21.4501(12)	23.8872(14)	24.385(4)
β (deg)	105.891(1)	105.144(1)	106.956(17)
V (Å^3)	4543.9(4)	7593.6(8)	8253(2)
Z	4	4	4
d_{calcd} (Mg/m^3)	1.730	1.468	1.469
scan mode	ω and ϕ	ω and ϕ	φ
F(000)	2332	3352	3646
abs coeff (mm^{-1})	3.824	2.361	2.388
θ range	1.57 to 27.50°	1.59 to 27.50°	2.20 to 25.00°
limiting indices	$-17 \le h \le 17$	$-15 \le h \le 17$	$-26 \le h \le 26$
	$-19 \le k \le 21$	$-31 \le k \le 30$	$-9 \le k \le 18$
	$-27 \le l \le 27$	$-30 \le l \le 31$	$-26 \le l \le 27$
reflns collected	31 120	51 437	25 542
independent reflns	10 206	17 013	11 804
min/max transm ratio	0.599	0.824	0.6467 and 0.5344
data/restraints/param	10 206/0/542	17 013/0/824	11 804/0/884
GOF on F^2	1.143	1.091	1.018
final *R* indices [$I > 2\sigma(I)$]	R1 = 0.0522	R1 = 0.0615	R1 = 0.0661
	wR2 = 0.1492	wR2 = 0.2045	wR2 = 0.1594
R indices (all data)	R1 = 0.0704	R1 = 0.0836	R1 = 0.1077
	wR2 = 0.1598	wR2 = 0.2159	wR2 = 0.1764

[a] $R1 = \sum||F_o| - |F_c||/\sum|F_o|$; $wR2 = (\sum[w(F_o^2-F_c^2)^2]/\sum[F_o^4])^{1/2}$; weight $= 1/[\sigma^2(F_o^2) + (AP)^2 + (BP)]$ where $P = (\max(F_o^2, 0) + 2F_c^2)/3$; $A = 0.0890$ and $B = 11.4580$ for **1**, $A = 0.1329$ and $B = 25.1908$ for **2b**, and $A = 0.0910$ and $B = 0$ for **6c**.

refinement cycles. Two sets of metal atoms (Pt1/Pd1 and Pd2/Pt2) were restraint to identical atom positions and thermal parameters. Relaxing the restraints led to unreasonable thermal parameters. All non-hydrogen atoms were refined anisotropically. Hydrogen atoms were included in calculated positions and refined using a riding model. Hydrogen atoms for the solvent molecule were omitted.

Crystals of **2b**·CH_2Cl_2 were grown from CH_2Cl_2/heptane at 20 °C. Single crystals were mounted on the same diffractometer and analyzed in the same way as **1**. The data were reduced (SAINT)[14] and corrected for absorption (SADABS).[15] All non-hydrogen atoms were refined anisotropically with the exception of the solvent molecule, which was refined isotropically. Hydrogen atoms were included in calculated positions and refined using a riding model.

Crystals of **6c**·$3.25CH_2Cl_2$·$0.5C_4H_{10}$ were grown from CH_2Cl_2/pentane at 20 °C. Single crystals were coated with perfluoroalkyl ether oil (ABCR), mounted using a glass fiber, and frozen in the cold nitrogen stream of the goniometer. The data were collected on a Stoe IPDS diffractometer. The data were reduced (Integrate in IPDS) and corrected for absorption (FACEIT in IPDS). The structure was solved by direct methods and refined by full-matrix least squares on F^2 (SHELXTL).[16] The metal atom positions were disordered over two sites and the occupancies determined using an isotropic model as 0.65 (Ptb and Pda) and 0.35 (Pta and Pdb) and fixed in subsequent refinement cycles. All non-hydrogen atoms except Pda and Pdb were refined anisotropically. Hydrogen atoms were included in calculated positions and refined using a riding model. Crystal and refinement data for **1**, **2b**, and **6c** are given in Table 1.

Results and Discussion

Structural Characterization of 1. The starting material **1** has been prepared according to the literature procedure,[8] and the structure was obtained by single-crystal X-ray crystallography (Table 2 and Figure 1). The overall geometry is isostructural to the $[M_2(\mu\text{-dppm})_2Cl_2]$ homonuclear dimers (M = Pd, Pt). The Pd−Pt bond length of 2.6487(4) Å corresponds within experimental error to those of [ClPd(μ-

Table 2. Selected Bond Distances (Å) and Angles (deg) for **1**[a]

Pt1−Pd2	2.649(4)	Pt1−P3	2.259(2)
Pt1−Cl1	2.415(2)	Pd2−P2	2.289(2)
Pd2−Cl2	2.430(2)	Pd2−P4	2.301(2)
Pt1−P1	2.275(2)		
Cl1−Pt1−Pd2	174.56(4)	P1−Pt1−Cl1	94.59(6)
Cl2−Pd2−Pt1	178.34(4)	P3−Pt1−Cl1	91.55(6)
P3−Pt1−P1	172.66(5)	P2−Pd2−Cl2	89.60(5)
P2−Pd2−P4	175.06(5)	P4−Pd2−Cl2	91.28(5)

[a] This is the structure with the highest occupancies. The other structure can be found in the Supporting Information.

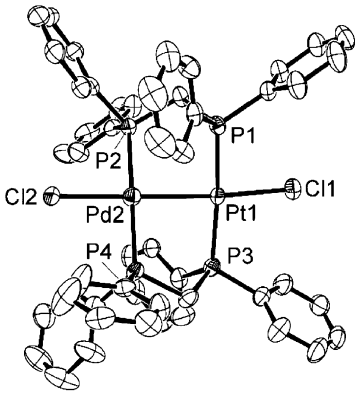

Figure 1. ORTEP plot of **1**. The ellipsoids are shown at 30% probability. The H atoms are omitted for clarity. This is one of two disordered forms (see the Experimental Section).

Scheme 1

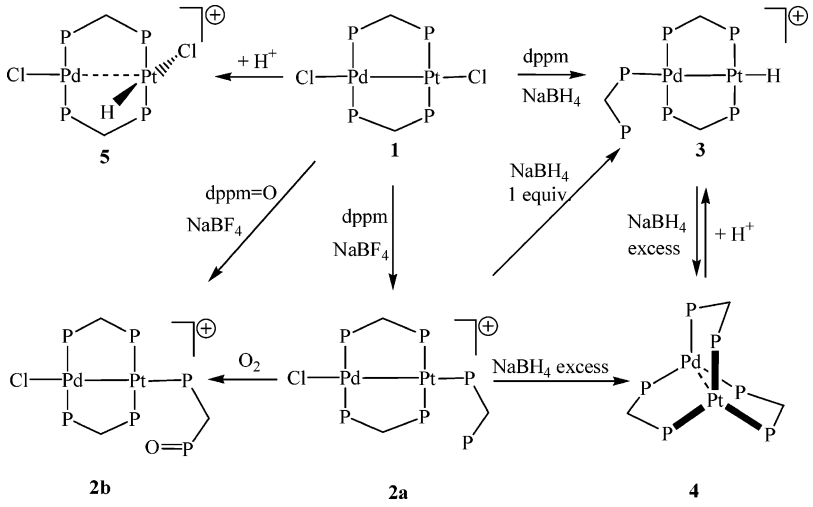

Scheme 2

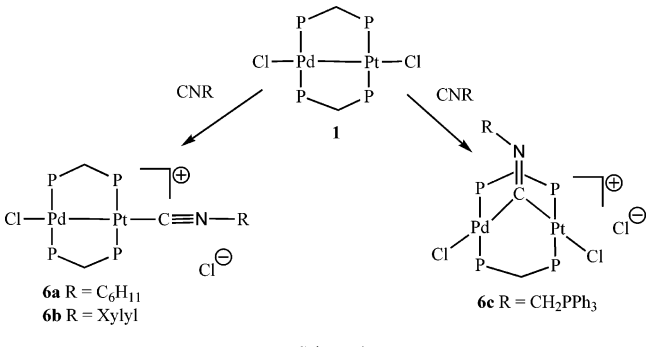

dppm)$_2$PdCl] [2.661(1) Å][17] and [ClPt(μ-dppm)$_2$PtCl] [2.651(1) Å],[18] and it also parallels that of [ClPt(μ-dppm)$_2$Pd(C_6F_5)] [2.643(1) Å].[19] The Pd(μ-dppm)$_2$Pt fragment forms two fused five-membered rings, adopting a chair conformation. The P1−Pt1−Pd2−P4, P1−Pt1−Pd2−P2, P3−Pt1−Pd2−P4, and P3−Pt1−Pd2−P2 torsion angles are 141.2, 33.9, 43.4, and 141.6°, respectively, and the Pd−P, Pt−P, and Pd−Cl bond lengths are normal (Table 2). The Pt−Cl bond distance of 2.415(2) Å is somewhat shorter than that of [ClPt(μ-dppm)$_2$Pd(C_6F_5)] [2.444(4) Å].

Reactivity of 1 toward Phosphines. The chemical reactivity of **1** toward free dppm, dppm═O, H^+, $NaBH_4$ (Scheme 1), and isocyanides (Scheme 2) has been explored. To test the site selectivity of **1** toward phosphine ligands, dppm was added in slight excess in the presence of $NaBF_4$ to provide **2a** in good yield.

The $^{31}P\{^1H\}$ NMR spectrum exhibits four sets of resonances for the chemically nonequivalent ^{31}P atoms consistent with axial substitution at the Pt center. It is interesting to note that no substitution occurs between [Pd_2(μ-dppm)$_2Cl_2$] and dppm, while [Pt_2(μ-dppm)$_2Cl_2$] does react similarly to **1**. The coupling constants ($^1J_{Pt-PA}$ = 2930 Hz, $^1J_{Pt-PC}$ = 2121 Hz, and $^2J_{PC-PD}$ = 54 Hz) agree with the literature data for species such as [Pt_2(μ-dppm)$_2$Cl(η^1-dppm)]$^+$ ($^1J_{Pt-PA}$= 2885 Hz and $^1J_{Pt-PC}$ = 2155 Hz)[20] and [Pt_2(μ-dppm)$_2$Cl(PPh_3)]$^+$ ($^1J_{Pt-PA}$ = 2856 Hz and $^1J_{Pt-PC}$ = 2207 Hz).[21] The resonance of the uncoordinated phosphorus P_D of the pendent dppm gives rise to a doublet at δ −26.7, quite close to the chemical shift found for free dppm (δ −21.3). The experimental spectrum has been successfully simulated, and the simulated spectrum corroborates that the two different sets of phosphorus nuclei of the bridging dppm exhibit an AA′BB′ spin system (see the Supporting Information for the labeling scheme of the phosphorus nuclei).

Compound **2a** is air-stable in the solid state; however, slow oxidation of the pendent phosphorus occurs in solution upon exposure to air to give the oxidized form **2b**.[22] This cationic compound was independently prepared by the addition of dppm═O to a slurry of **1** and $NaBF_4$ in THF. According to the $^{31}P\{^1H\}$ NMR spectrum (see the Experimental Section), exclusive substitution of the Pt-bound chloro ligand by dppm═O took place. The question arises as to why the displacement reaction of Cl^- by dppm and dppm═O takes place at platinum rather than palladium. Substitution reactions at Pd are known to be much faster than those at Pt, but the positive charge of the resulting cationic salts **2a** and **2b** is probably better stabilized on the more electron-rich Pt^I center. Furthermore, generation of a new Pt−P bond instead of a Pd−P bond may also be more favorable for thermodynamic reasons because a Pt−P bond is known to be more stable than a Pd−P bond. This argument is corroborated by Braunstein's findings that, upon a substitution reaction of **1** with metalates L_nM^- at the M−Cl bond, a subsequent migration of the more labile Pd-bound dppm phosphorus to

(17) Besenyei, G.; Parkanyi, L.; Gacs-Baitz, E.; James, B. R. *Inorg. Chim. Acta* **2002**, *327*, 179.
(18) (a) Brown, M. P.; Puddephatt, R. J.; Rashidi, M.; Manojlovic-Muir, L. J.; Muir, K. W.; Solomun, T.; Seddon, K. R. *Inorg. Chim. Acta* **1977**, *23*, L33. (b) Manojlovic-Muir, L. J.; Muir, K. W.; Solomun, T. *Acta Crystallogr., Sect. B: Struct. Sci.* **1979**, *B35*, 1237.
(19) Fornies, J.; Martinez, F.; Navarro, R.; Redondo, A.; Tomas, M.; Welch, A. J. *J. Organomet. Chem.* **1986**, *316*, 351.
(20) Krevor, J. V. Z.; Yee, L. *Inorg. Chem.* **1990**, *29*, 4305.
(21) Krevor, J. V. Z.; Simonis, U.; Richter, J. A., II. *Inorg. Chem.* **1992**, *31*, 2409.
(22) Some researchers suggested that the oxidation of phosphines may also be due to the action of peroxides contained in the crystallization solvent. Such a type of oxidative behavior for solvent-contained peroxides has recently been described. See: Sevillano, P.; Habtemariam, A.; Castineiras, A.; Garcia, M. E.; Sadler, P. J. *Polyhedron* **1999**, *18*, 383.

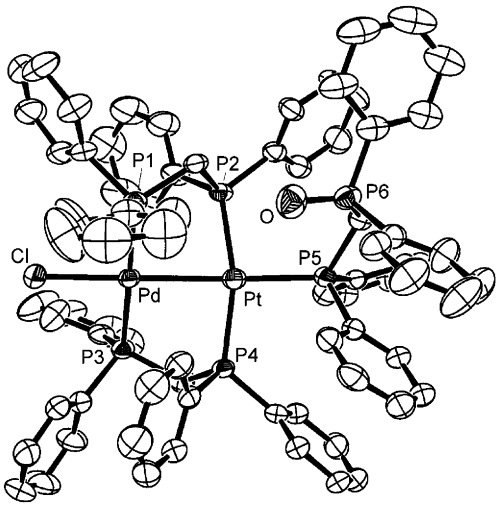

Figure 2. ORTEP plot of **2b**. The ellipsoids are shown at 30% probability. The H atoms and counterion are omitted for clarity.

Table 3. Selected Bond Distances (Å) and Angles (deg) for **2b**

Pd−Pt	2.691(1)	Pt−P4	2.310(2)
Pd−P1	2.295(2)	Pd−Cl	2.409(2)
Pd−P3	2.290(2)	Pt−P5	2.343(2)
Pt−P2	2.286(2)	P6−O	1.422(7)
Cl−Pd−Pt	175.71(6)	P1−Pd−Cl	88.96(7)
P5−Pt−Pd	170.61(5)	P3−Pd−Cl	90.34(7)
P3−Pd−P1	179.03(7)	P2−Pt−P5	98.17(6)
P2−Pt−P4	163.04(6)	P4−Pt−P5	97.91(6)
P5−C63−P6	118.45(7)		

M takes places, thus leading to a dppm-spanned triangular Pd−Pt−M core.[9c,h]

Consistent with the ^{31}P NMR findings, the coordination of dppm═O at the Pt center via a P−Pt bond has, furthermore, been confirmed by an X-ray structure determination conducted on an orange single crystal (Figure 2). As expected, the core structure is quite similar to that of **1**, except that the dppm−P atom is bonded at the Pt center. The Pd−Pt bond distance of 2.6969(6) Å is slightly longer than that found for **1**. The P−Pd−Pt−P dihedral angles are 36.8 and 44.4°, similar to that found for **1**, and the other core distances are normal (Table 3). The η^1-dppm oxide adopts a "U-shaped" conformation, where the O atom is oriented almost above the Pt center, but the long distance (3.765 Å) excludes any bonding interaction.

FT Raman and UV−Vis Characterization of the Pd−Pt Bond. The FT Raman spectra of **1** and **2a** depicted in Figure 3 exhibit strong scatterings associated with ν(Pd−Pt) at 154 and 138 cm^{-1}, respectively. The text below and Table 3[17,18,23−35] compare various d(M−M′) and ν(M−M′)

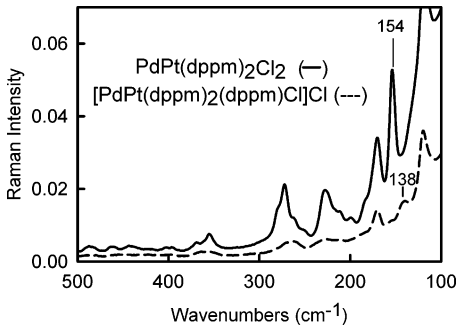

Figure 3. FT Raman spectra in the 100−500-cm^{-1} region of **1** (—) and **2a** (− − −) in the solid state. Resolution: 2 cm^{-1}, 10 000 scans. The intensity of the scattering has not been modified in this figure.

Table 4. d(M−M′) and ν(M−M′) for Various d^9−d^9 Pd_2-, Pt_2-, and PdPt-Bonded Bimetallics

compound	d(M−M′)/Å	ν(M−M′)/cm^{-1}	ref
$[PdPt(dppm)_2Cl_2]$	2.648(1)	154	this work
$[PdPt(dppm)_2(\eta^1\text{-dppm})Cl]^+$	2.697(1)	138	this work
$[PdPt(CNMe)_6]^{2+}$		160	31
$[Pd_2(dppm)_2Cl_2]$	2.661(1)	152	17, 29
$[Pd_2(CNMe)_6]^{2+}$	2.531(1)	163	26, 27
$[Pt_2(dppm)_2Cl_2]$	2.651(1)	150	18, 29
$[Pt_2(CNMe)_6]^{2+}$		153	31

for several d^9−d^9 Pd_2-, Pt_2-, and PdPt-bonded bimetallics and reveal an inverse relationship between d(M−M′) and ν(M−M′).

The frequency for **1** (154 cm^{-1}) resembles that of those reported for the $M_2(\mu\text{-dppm})_2Cl_2$ complexes (M = Pd, 152 cm^{-1}; Pt, 150 cm^{-1}). Because the d(M_2) values are similar, the d(Pd−Pt) must be close as well. The lower ν(Pd−Pt) vibration for **2a** is consistent with the longer bond and the increase in mass along the X−M−M′−X axis in which the ν(M−M′), ν(M−X), and ν(M′−X) modes are strongly coupled.[36] For instance, the $\nu(Pd_2)$ values for the series $[Pd_2(\mu\text{-dmb})_2Cl_2]$ (171 cm^{-1};[23] dmb = 1,8-diisocyano-*p*-menthane) = $[Pd_2(CN\text{-}t\text{-}Bu)_4Cl_2]$[24] (170 cm^{-1})[25] > $[Pd_2(CNMe)_6]^{2+}$[26] (163 cm^{-1}),[27] the sequence $[Pd_2(\mu\text{-dppm})_2Cl_2]$[17] (152 cm^{-1}) > $[Pd_2(\mu\text{-dppm})_2(SnCl_3)Cl]$[28] (147 cm^{-1}) > $[Pd_2(\mu\text{-dppm})_2(SnCl_3)_2]$ (140 cm^{-1}),[29] and the pair $[Pd_3(CNMe)_8]^{2+}$ (114 cm^{-1}) > $[Pd_3(CNMe)_6(PPh_3)_2]^{2+}$[30] (90 cm^{-1})[31] fully demonstrate this effect. Other related examples involving d^9−d^9 X−M−M−X systems, such as the $[Pd_2(\mu\text{-diphos})_2X_2]$ [diphos = dppm;[29,32] dmpm[33] = bis(dimethylphosphino)methane], $[Pd_2(\mu\text{-dmb})_2X_2]$,[23] and $[Pt_2(\mu\text{-dppm})_2X_2]$ (X = Cl, Br, I),[18,29,34] also exist.

The UV−vis spectra for **1** and **2a** in chloroform and acetone, respectively, at 293 K exhibit low-energy maxima

(23) Perreault, D.; Drouin, M.; Michel, A.; Harvey, P. D. *Inorg. Chem.* **1992**, *31*, 2740.
(24) (a) Yamamoto, Y.; Yamazaki, H. *Bull. Chem. Soc. Jpn.* **1985**, *58*, 1843. (b) Yamamoto, Y.; Takahashi, K.; Yamazaki, H. *Bull. Chem. Soc. Jpn.* **1987**, *60*, 2665.
(25) Sicard, S.; Harvey, P. D., unpublished results, 2003.
(26) (a) Goldberg, S. Z.; Eisenberg, R. *Inorg. Chem.* **1976**, *15*, 535. (b) Doonan, D. J.; Balch, A. L.; Goldberg, S. Z.; Eisenberg, R.; Miller, J. S. *J. Am. Chem. Soc.* **1975**, *97*, 1961.
(27) Garciafigueroa, E.; Sourisseau, C. *New J. Chem.* **1978**, *2*, 593.
(28) Olmstead, M. M.; Benner, L. S.; Hope, H.; Balch, A. L. *Inorg. Chim. Acta* **1979**, *32*, 193.
(29) Alves, O. L.; Vitorge, M. C.; Sourisseau, C. *New J. Chem.* **1983**, *7*, 231.
(30) Balch, A. L.; Boehm, J. R.; Hope, H.; Olmstead, M. M. *J. Am. Chem. Soc.* **1976**, *98*, 7431.
(31) Clark, R. J. H.; Sourisseau, C. *New J. Chem.* **1980**, *4*, 287.
(32) Perreault, D.; Drouin, M.; Michel, A.; Harvey, P. D. *Inorg. Chem.* **1993**, *32*, 1903.
(33) Kullberg, M. L.; Lemke, F. R.; Powell, D. R.; Kubiak, C. P. *Inorg. Chem.* **1985**, *24*, 3589.
(34) Harvey, P. D.; Truong, K. D.; Aye, K. T.; Drouin, M.; Bandrauk, A. D. *Inorg. Chem.* **1994**, *33*, 2347.
(35) Sourisseau, C.; Hervieu, J.; Vitorge, M.-C. *Spectrochim. Acta, Part A* **1980**, *36A*, 153.
(36) Herzberg, G. *Molecular Spectra and Molecular Structure*; Van Nostrand: New York, 1945; Vol. II, p 180.

(λ_{max}) at 420 and 366 nm ($\epsilon = 6274\ M^{-1}\ cm^{-1}$). These bands are associated with the dσ−dσ* transition, typical for d^9−d^9 M_2-bonded Pd and Pt dimers.[37] For the homonuclear Pd_2- and $Pt_2(\mu\text{-dppm})_2Cl_2$ complexes, the λ_{max} values are found at 418 nm (2-methyltetrahydrofuran, 2-MeTHF)[37b] and 423 nm (CH_2Cl_2),[29] respectively.

Treatment of **2a** with just 1 equiv of $NaBH_4$ causes a migration of the dangling dppm ligand from Pt to Pd upon exchange of Cl^- by H^-, leading to the hydride complex **3** (Scheme 1). **3** is characterized by a ^1H NMR spectrum that exhibits a hydride signal in the form of a broadened doublet at δ −6.45 (the full width at half-maximum is 20.5 Hz; see the Supporting Information) with unresolved cis couplings, consistent with a T-shaped $HPtP_2$ fragment ($^1J_{Pt-H} = 706.6$ Hz and $^3J_{H-P(trans)} = 165.0$ Hz). Although the $^1J_{Pt-H}$ magnitude is quite low for a terminal $^1J_{Pt-H}$ coupling, there are some precedents. A $^1J_{Pt-P}$ coupling of 713 Hz has been measured for $[(OC)_4Fe(\mu\text{-dppm})Pt(H)PPh_3]^+$.[38] The diplatinum analogue of **3** $[HPt(\mu\text{-dppm})_2Pt(\eta^1\text{-dppm})]^+$ was reported 20 years ago,[39] but in this case, a rapid dynamic process in which the two P atoms of the dangling dppm exchange exists. However, the low-temperature NMR data agree with those found for **3** [δ_H −8.4 (broad signal), $^1J_{Pt-H} = 980$ Hz, $^3J_{H-P} = 45$ Hz].

Reduction of **2a** in THF with an excess of $NaBH_4$ affords the orange mixed-metal complex **4** (Scheme 1). This d^{10}−d^{10} species, which degrades rapidly upon exposure to air, was identified by ^{31}P NMR, FABMS, and UV−vis spectroscopy. As is expected for a Pt^0 center, the $^1J_{Pt-P}$ coupling constant has considerably increased with a magnitude almost identical with that of $[Pt_2(\mu\text{-dppm})_3]$ (4430 vs 4455 Hz).[40b] The UV−vis spectrum exhibits a strong absorption at 460 nm associated with a d$\sigma \rightarrow$ dσ* electronic transition ($\epsilon = 10159\ M^{-1}\ cm^{-1}$), which falls between the corresponding absorptions for the homodinuclear $[Pd_2(\mu\text{-dppm})_3]$ (420 nm) and $[Pt_2(\mu\text{-dppm})_3]$ (479 nm) counterparts.[40,41] **4** is also found to be luminescent in 2-MeTHF glasses ($\lambda_{emi} = 724$ nm; $\tau_e = 12 \pm 1$ μs, 77 K). **4** can alternatively be obtained from **3** by reduction with an excess of $NaBH_4$. Inversely, the addition of an excess of formic acid (10 equiv in the presence of $NaBF_4$) to **4** leads to **3**. The preference for Pt vs Pd as the protonation site may have its origin in the better stabilization of the positive charge on the more electron-rich platinum center and the formation of a stronger Pt−H bond compared to a Pd−H bond.[6a]

Chart 1

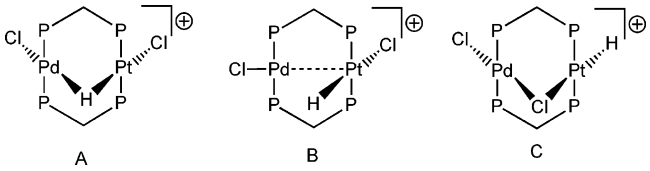

The cationic hydride complex **5** was prepared by adding HPF_6 or HBF_4 to a dichloromethane solution of **1**. It was characterized by LSIMS (MALDI-TOF), elemental analysis, and NMR spectroscopy. The ^1H NMR spectrum exhibits an apparent broadened quintet resonance at δ −15.56 with a $^2J_{P-H}$ coupling of 8 Hz and a $^1J_{Pt-H}$ coupling of 888 Hz. A priori, a structural description of **5** possessing a bridging hydride could be envisaged (isomer A in Chart 1). This μ-bonding mode has been proposed by Brown et al. for the homodinuclear complex $[ClPt(\mu\text{-dppm})_2(\mu\text{-H})PtCl][PF_6]$ (δ_H −16.60 (quintet); $^1J_{Pt-H} = 810$ Hz).[42] At first glance, the chemical shift and magnitude of the $^1J_{Pt-H}$ coupling constant (888 Hz) of **5** compare favorably with that compound.

However, a $^1J_{Pt-H}$ coupling of 888 Hz is far beyond the typical range of ca. 300−600 Hz for bridging hydrides in heterometallic systems and is much closer to that reported for numerous mononuclear and heterodinuclear Pt complexes with a terminal hydride ligand (ca. 770−1200 Hz; see also compound **3**). Examples are $[Pt(PMePh_2)_2(H)Cl]$ (1260 Hz), $[Pt(PPh_3)_3(H)]^+$ (771 Hz),[43a] $[Pt(PMePh_2)_3(H)]^+$ (840 Hz),[43b] $[(OC)_3W(\mu\text{-dppm})_2Pt(H)Cl]$ (1102 Hz),[44a] $[(OC)_2ClFe(\mu\text{-dppm})_2Pt(H)Cl][PF_6]$ (δ_H −17.0, apparent quintet; $^1J_{Pt-H} = 860$ Hz),[45a] and $[(OC)_4Fe(\mu\text{-}PPh_2)Pt(H)(CO)(PCy_3)]$ ($^1J_{Pt-H} = 980$ Hz).[45b] In contrast, the heterometallic alkyls and aryls of the type $[RPt(\mu\text{-dppm})_2(\mu\text{-H})PtR][PF_6]$, for which the existence of a μ-hydride was ascertained unambiguously by X-ray diffraction studies, exhibit all $^1J_{Pt-H}$ couplings in the expected range of ca. 500 Hz.[10] Note that Brown et al. have also determined a $^1J_{Pt-H}$ coupling of 540 Hz for the μ-hydride ligand of $[HPt(\mu\text{-dppm})_2(\mu\text{-H})PtH][PF_6]$, whereas the two terminal hydrides give rise to a $^1J_{Pt-H}$ coupling of 1138 Hz.[42] Taking into account these data, the presence of a terminal

(37) For instance, see: (a) Harvey, P. D.; Murtaza, Z. *Inorg. Chem.* **1993**, *32*, 4721. (b) Meilleur, D.; Harvey, P. D. *Can. J. Chem.* **2001**, *79*, 552.

(38) Fontaine, X. L. R.; Jacobsen, G. B.; Shaw, B. L.; Thornton-Pett, M. *J. Chem. Soc., Dalton Trans.* **1988**, 741.

(39) (a) Brown, M. P.; Fisher, J. R.; Hill, R. H.; Puddephatt, R. J.; Seddon, K. R. *Inorg. Chem.* **1981**, *20*, 3516. (b) Manojlovic-Muir, L.; Muir, K. W. *J. Chem. Soc., Chem. Commun.* **1982**, 1155. (c) Al-Resayes, S. I.; Hitchcock, P. B.; Nixon, J. F. *J. Organomet. Chem.* **1984**, *267*, C13. (d) Azam, K. A.; Brown, M. P.; Hill, R. H.; Puddephatt, R. J.; Yavari, A. *Organometallics* **1984**, *3*, 697.

(40) (a) Grossel, M. C.; Brown, M. P.; Nelson, C. D.; Yavari, A.; Kallas, E.; Moulding, R. P.; Seddon, K. R. *J. Organomet. Chem.* **1982**, *232*, C13. (b) Manojlovic-Muir, L.; Muir, K. W.; Grossel, M. C.; Brown, M. P.; Nelson, C. D.; Yavari, A.; Kallas, E.; Moulding, R. P.; Seddon, K. R. *J. Chem. Soc., Dalton Trans.* **1986**, 1955. (c) Harvey, P. D.; Gray, H. B. *J. Am. Chem. Soc.* **1988**, *110*, 2145. (d) Harvey, P. D.; Dallinger, R. F.; Woodruff, W. H.; Gray, H. B. *Inorg. Chem.* **1989**, *28*, 3057.

(41) An emission band is observed at 724 nm for **4** (77 K; 2-MeTHF), which falls between the $[Pd_2(dppm)_3]$ (680 nm) and $[Pt_2(dppm)_3]$ (800 nm) luminescences. The emission lifetime is 12 ± 1 μs, which compares more to that measured for $[Pt_2(dppm)_3]$ at 77 K (10.6 ± 0.2 μs) than to that for $[Pd_2(dppm)_3]$ (107 ± 1 μs). This result is consistent with the effect of spin−orbit coupling, which is dominant for Pt.

(42) (a) Brown, M. P.; Puddephatt, R. J.; Rashidi, M.; Seddon, K. R. *J. Chem. Soc., Dalton Trans.* **1978**, 516. (b) Brown, M. P.; Fisher, J. R.; Franklin, S. J.; Puddephatt, R. J.; Seddon, K. R. *J. Organomet. Chem.* **1978**, *161*, C46.

(43) (a) Chinakov, V. D.; Il'inich, G. N.; Zudin, V. N.; Likholobov, V. A.; Nekipelov, V. M. *J. Organomet. Chem.* **1989**, *366*, 421. (b) Appleton, T. G.; Clark, H. C.; Manzer, L. E. *Coord. Chem. Rev.* **1973**, *10*, 355.

(44) (a) Blagg, A.; Shaw, B. L. *J. Chem. Soc., Dalton Trans.* **1987**, 221. In refs 44a and 44b, the phenomenon of reversible bridged-terminal hydrido equilibria in W−Pt and Fe−Pt is discussed. A similar equilibration between a bridged and terminal hydride bonding mode cannot be ruled out for compound **5**. (b) Powell, J.; Gregg, M. R.; Sawyer, J. F. *J. Chem. Soc., Chem. Commun.* **1987**, 1029.

(45) (a) Braunstein, P.; Faure, T.; Knorr, M. *Organometallics* **1999**, *18*, 1791. (b) Powell, J.; Gregg, M. R.; Sawyer, J. F. *Inorg. Chem.* **1989**, *28*, 4451.

Chart 2

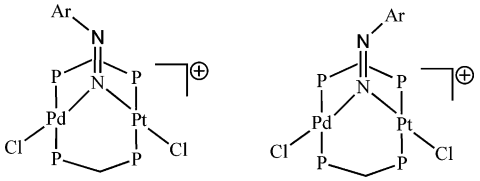

hydride ligand in **5** is more likely (B or C) [IR: 1954 cm^{-1}, ν(Pt−H)].[44b]

Reactivity of 1 toward Isocyanides. Upon the addition of 1 equiv of cyclohexyl isocyanide to a CH_2Cl_2 solution of **1**, the Pt-bound chloro ligand is rapidly substituted by CNR, giving exclusively the cationic complex **6a** (Scheme 2). The *terminal* bonding mode of the isocyanide can be deduced from the IR spectrum, which displays a ν(C≡N) stretch at 2197 cm^{-1}. This bonding mode contrasts with that reported by Balch for the reaction of [ClPd(μ-dppm)$_2$PdCl] with CNC_6H_{11}. In the latter case, the isocyanide-bridged A-frame complex [ClPd(μ-dppm)$_2$(μ-CNC_6H_{11})PdCl] was obtained [ν(C═N) = 1645 cm^{-1}].[46a]

For comparison, we also reacted [ClPd(μ-dppm)$_2$PdCl] and **1** with the less nucleophilic xylyl isocyanide in a CH_2Cl_2 solution. Again, the Pd dimer gave exclusively the red A-frame compound [ClPd(μ-dppm)$_2$(μ-C═N−xylyl)PdCl] [ν(C═N) = 1685 cm^{-1}], whereas in the case of **1**, the yellow cationic complex **6b** was isolated. The ^{195}Pt{^{1}H} NMR of **6b** consists of a broadened triplet-of-triplet resonance centered at δ −2407 with $^1J_{Pt-P}$ couplings of 2590 Hz and $^{2+3}J_{Pt-P}$ of 126 Hz. These couplings are also found in the ^{31}P resonance (AA′BB′) centered at δ −3.7 with N = 88 Hz ($N = |^2J(P_AP_B) + {}^4J(P_AP_{B'})|$). However, the bonding mode of the CNR ligand switches from *terminal* to *bridging* when the cationic phosphonium salt [C≡NCH_2PPh_3]Cl is treated in a 1:1 ratio with **1** in a CH_2Cl_2 solution. In this case, the yellow air-stable A-frame compound **6c** was isolated in almost quantitative spectroscopic yield. The ^{195}Pt{^{1}H} NMR of **6c** gives rise to a triplet of triplets centered at δ −2306. Compared to the $^1J_{Pt-P}$ and $^{2+3}J_{Pt-P}$ couplings of **6b**, those of **6c** have considerably increased to 3383 and 423 Hz, with the latter being now a pure $^3J_{Pt-P}$ coupling constant. In addition to the ^{31}P resonances due to the metal-bound phosphorus nuclei (AA′XX′ spin system) centered at δ 11.8, a singlet resonance at δ 15.9 stems from the phosphonium group. The observation of just one species in solution needs a comment: in a paper by Neve et al., the reaction of **1** with the aromatic diazonium salt [p-$FC_6H_4N_2$][BF_4] has been described.[47] To rationalize the observation of two species in solution, the existence of two isomers with different orientations of the bent bridging arenediazenido ligand has been suggested (Chart 2). In the case of **6c**, a rapid "windscreen-wiper" motion of the bent CNR ligand or exclusive formation of just one isomer may account for the spectroscopic data.

Crystal Structure of 6c. The insertion of [C≡NCH_2PPh_3]-Cl into the Pd−Pt bond has also been confirmed by an X-ray diffraction study (Figure 4). The overall structure of **6c** resembles that of the Pd_2 A-frame complex [ClPd(μ-dppm)$_2$-(μ-C═NPh)PdCl].[46b] Like in the latter compound [d(Pd···Pd) = 3.188(1) Å], insertion causes a considerable elongation of the metal−metal interaction [d(Pd···Pt) = 3.228(8) Å]. The bending of the angle C═NR is even more pronounced [117.0(9) vs 129.3(9)°]. The coordination spheres around Pd and Pt are square planar and meet at the bridging C1 atom, which spans in a symmetric manner the two metal centers (Table 5).

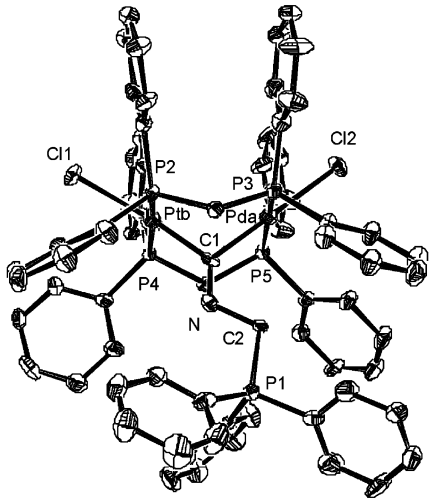

Figure 4. ORTEP plot of **6c**. The ellipsoids are shown at 30% probability. The H atoms and counterion are omitted for clarity. The figure shows the disordered form with 0.65 Ptb and Pda site occupancies (see the Experimental Section).

Table 5. Selected Bond Distances (Å) and Angles (deg) for **6c**

Ptb−C1	2.004(11)	Ptb−P4	2.294(5)
Pda−C1	1.993(13)	Pda−P3	2.321(8)
C1−N	1.252(12)	Pda−P5	2.332(6)
Pda−Cl2	2.419(8)	Ptb−P2	2.338(5)
Ptb−Cl1	2.399(4)	C2−N	1.474(14)
Cl1−Ptb−C1	179.2(4)	P2−Ptb−Cl1	94.2(2)
Cl2−Pda−C1	178.5(5)	P4−Ptb−Cl1	92.1(2)
P4−Ptb−P2	172.1(2)	P5−Pda−Cl2	91.7(3)
P5−Pda−P3	171.6(4)	P3−Pda−Cl2	94.8(3)
Pda−C1−Ptb	107.7(5)	P3−C33−P2	115.2(4)
P4−C58−P5	116.6(6)	N−C2−P1	109.7(7)

The preference of [C≡NCH_2PPh_3]Cl to adopt a bridging bonding mode may be rationalized by its strong π-acceptor propensity (due to the positive charge), which excels that of xylyl isocyanide. These findings are completely in line with the recent reactivity studies on the early−late couple [(OC)$_4$W(μ-CO)(μ-Ph_2PXPPh_2)Pt(PPh_3)] (X = NH, CH_2) toward various isocyanides with diverging electronic and steric properties.[48] These examples nicely illustrate again that different reactivity patterns can be expected using heterobimetallic d^9−d^9 systems instead of homobimetallic ones.

Electrochemistry of 1−5. Compound **1** exhibits a reduction wave, A, at −1.38 V vs SCE on the rotating disk electrode (RDE) voltammogram (Figure 5, trace a_1). This

(46) (a) Benner, L. S.; Balch, A. L. *J. Am. Chem. Soc.* **1978**, *100*, 6099. (b) Khan, M. A.; McAlees, A. J. *Inorg. Chim. Acta* **1985**, *104*, 109. (c) Hanson, A. W.; McAlees, A. J.; Taylor, A. *J. Chem. Soc., Perkin Trans.* **1985**, 441.
(47) Neve, F.; Longeri, M.; Ghedini, M.; Crispini, A. J. *Inorg. Chim. Acta* **1993**, *205*, 15.
(48) (a) Knorr, M.; Strohmann, C. *Organometallics* **1998**, *18*, 248. (b) Knorr, M.; Jourdain, I.; Lentz, D.; Willemsen, S.; Strohmann, C. *J. Organomet. Chem.* **2003**, *684*, 216.

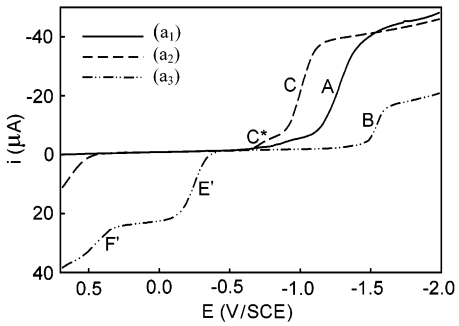

Figure 5. RDE voltammogram of **1** in THF with 0.2 M Bu_4NPF_6 as the supporting electrolyte: (a_1) **1** alone; (a_2) **1** with 3.4 equiv of dppm; (a_3) after bulk electrolysis at −1.2 V (n = 2 F mol^{-1}). Scan rate: 20 mV s^{-1}.

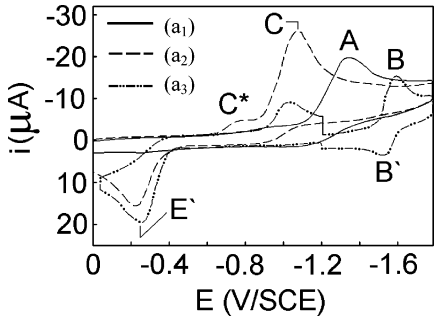

Figure 6. CV for **1** in THF with 0.2 M Bu_4NPF_6 as the supporting electrolyte: (a_1) **1** alone; (a_2) **1** with 3.4 equiv of dppm; (a_3) after bulk electrolysis at −1.2 V. Initial potential: (a_1 and a_2) 0 V; (a_3) −1.2 V. Scan rate: 100 mV s^{-1}.

reduction potential falls between the corresponding reductions for the homonuclear dimers [$Pd_2(\mu$-dppm$)_2Cl_2$] (−1.26 V vs SCE)[49] and [$Pt_2(\mu$-dppm$)_2Cl_2$] (−1.64 V vs SCE).[20] In CV, the corresponding reduction process A is irreversible (Figure 6, trace a_1), and bulk electrolysis at this peak potential leads to decomposition of **1** without the appearance of any well-defined product. In the presence of 3.4 equiv of dppm, an important change in the voltammograms is noticed. In the RDE voltammogram, wave A disappears, and a new reduction wave C at −1.02 V vs SCE sets in with a current intensity approximately the same as that of wave A. In addition, a small shoulder, C*, at −0.75 V vs SCE is also apparent (Figure 5, trace a_2). In CV, after reduction at the potential of peak C, only one well-defined reoxidation wave E′ is observed at −0.25 V vs SCE (Figure 6, trace a_3). The comparison with an authentic sample allows one to assign peak C to the presence of **2a** in the solution. The lower energy peak potential of peak C vs A (ΔE = 360 mV) is consistent with the cationic state of **2a**.

The bulk electrolysis of **2a** at −1.2 V vs SCE (at the potential of peak C) requires about 2 electrons to reach completion (n_{exp} = 1.9 F mol^{-1}). The resulting red-orange solution exhibits a reduction wave at −1.55 V vs SCE, B, but the current intensity is significantly lower than that observed for peak C. Two reoxidation waves are evident at −0.25, E′, and +0.46 V vs SCE, F′ (Figure 5, trace a_3). The intensities for waves B and F′ are very similar. These findings

(49) (a) Nemra, G.; Lemoine, P.; Braunstein, P.; de Méric de Bellefon, C.; Ries, M. *J. Organomet. Chem.* **1986**, *304*, 245. (b) Gauthron, I.; Mugnier, Y.; Hierso, K.; Harvey, P. D. *New J. Chem.* **1998**, *22*, 237.

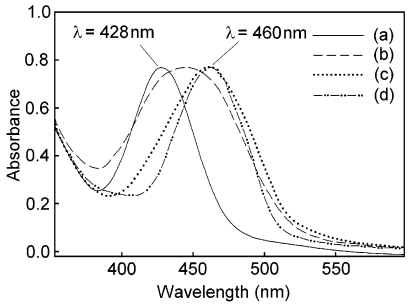

Figure 7. Monitoring of the reduction of **3** at −1.7 V by UV−vis spectroscopy: (a) **3** before electrolysis; (b) just before electrolysis; (c) after 30 min; (d) at completion, i.e., **4**.

indicate that two products are formed. By comparison with authentic samples, these peaks are associated with the presence of **3** and **4**, for the wave systems B/F′ and E′, respectively, and allow eq 1 to be written:

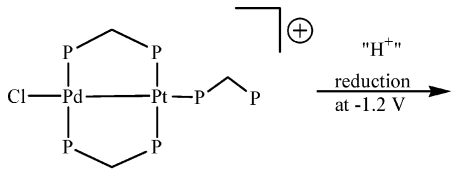

2a

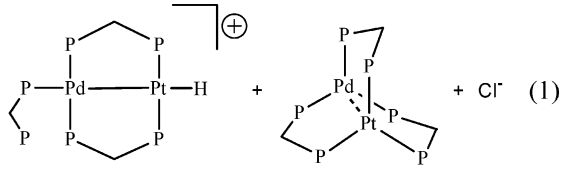

(1)

3 **4**

On the other hand, when the bulk electrolysis of **2a** is performed at −1.7 V vs SCE, it consumes about 2.8 electrons and only **4** is noticed in the resulting solution. This indicates that **3** is further reduced to produce **4**.

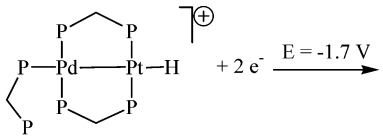

3

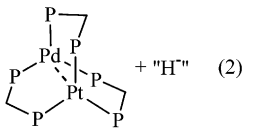

(2)

4

When the bulk electrolysis is monitored by UV−vis spectroscopy, it is possible to observe the conversion of **3** into **4**. The presence of a very large spectral envelope and the absence of isosbestic points are consistent with the presence of more than two species during the reaction (Figure 7).

The generation of **3** is surprising and suggests the presence of residual water in the solution, despite the precautions. To prove this hypothesis, a large excess of water was added to the starting solution of **2a** prior to electrolysis at −1.2 V vs

SCE. Indeed, in the presence of 20% of water, **3** is the only product observed, allowing one to write

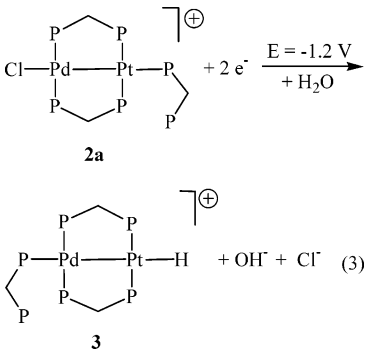

The number of electrons required to reach completion for eq 3 is 2 electrons, but 6.5 equiv is measured. This result suggests that a parallel catalytic process involving the presence of water operates. To verify this hypothesis, the addition of 4.7 equiv of the proton source HCO_2H to a solution containing **2a** was conducted. The bulk electrolysis performed at −1.2 V vs SCE also leads to **3** quantitatively. The amount of consumed electricity is 2 F mol^{-1} (n_{exp} = 1.99), in accordance with the following balanced equation:

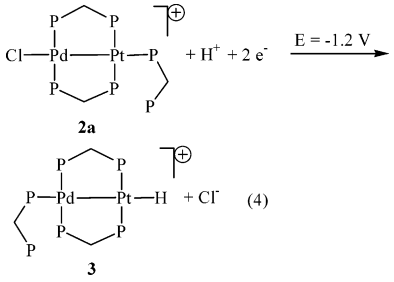

The reduction of **3** in the presence of 28 equiv of HCO_2H at the potential of peak B (−1.55 V vs SCE) leads expectedly to **4**, and the consumed number of electrons approaches 30 F mol^{-1}. This experiment confirms the presence of a catalytic process, presumably H_2 evolution based on our previous research on the related cluster $[Pd_4(dppm)_4(H)_2]^{2+}$,[50] hence affording a plausible explanation for the results described above on the residual water.

4 can be reoxidized at the potential of peak E′. In the presence of Cl^-, **2a** is fully recovered based on the relative intensity of the peak current before and after electrolysis:

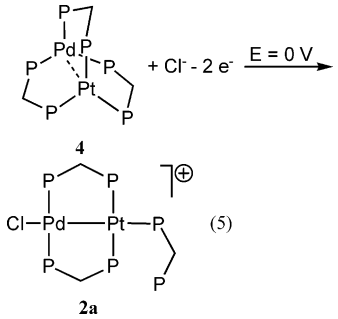

The addition of 2 equiv of formic acid to **4** causes the disappearance of the oxidation wave E′ and the appearance

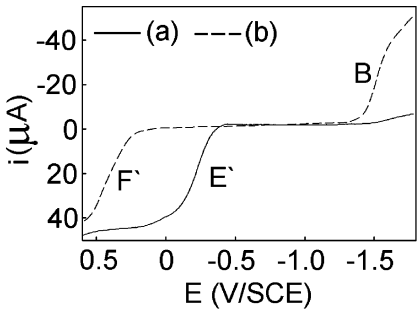

Figure 8. RDE voltammogram of **4** in THF in the presence 0.2 M Bu_4NPF_6: (a) **4** alone; (b) **4** in the presence of 2 equiv of HCO_2H. Scan rate: 20 mV s^{-1}.

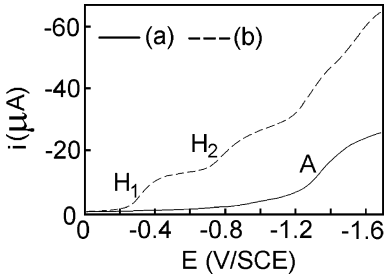

Figure 9. RDE voltammogram of **1** in THF in the presence of 0.2 M Bu_4NPF_6: (a) **1** alone; (b) **1** in the presence of 1.7 equiv of HPF_6. Scan rate: 20 mV s^{-1}.

of the waves B and F′ in the RDE voltammogram, characteristic of compound **3** (Figure 8) and consistent with Scheme 1 and the results described above. This reactivity is also observed with oxalic acid but not with acetic acid. This difference can be interpreted considering their acidity constants (p*K*: HOOC−COOH, 1.23; HCOOH, 3.8; CH_3COOH, 4.7).[51]

The addition of 1.7 equiv of HPF_6 to **1** induces the replacement of wave A by the waves H_1 and H_2 at −0.25 and −0.72 V, associated with complex **5** (Scheme 1), as verified with an authentic sample (Figure 9).[52] On the basis of the relative peak current, these H_1 and H_2 waves are assigned to two one-electron transfers. The electrochemical behavior of **5** is complex. On the basis of our recent work on $[Pd_4(dppm)_4(H)_2]^{2+}$,[50] one could expect a reductive elimination of H_2 after a one-electron reduction ($\mathbf{5} + 1e^- \rightarrow \mathbf{1} + {}^1/_2H_2$). However, this reactivity is not observed, suggesting that the stronger Pt−H interactions prevent H_2 elimination. We propose that the first intermediate formed by monoelectronic reduction at the potential of wave H_1 is **5′**. The reduction potential of this compound (wave H_2), which is unstable, is consistent with its cationic nature:

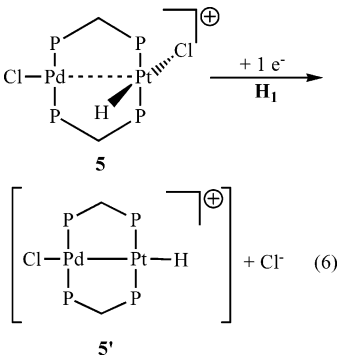

Scheme 3

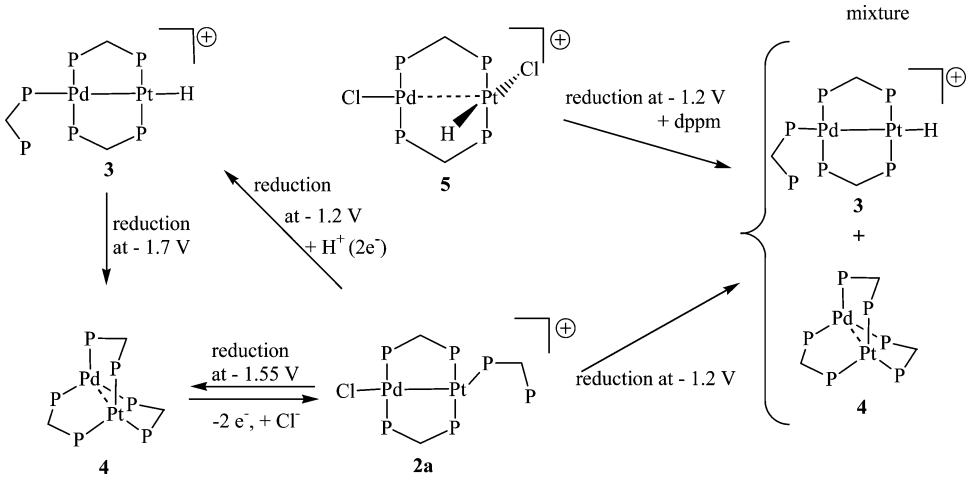

The addition of 3 equiv of dppm to **5** leads after reduction at −1.2 V vs SCE to **3** (waves B and F′) and **4** (wave E′) as major and minor products, respectively, according to the resulting CV:

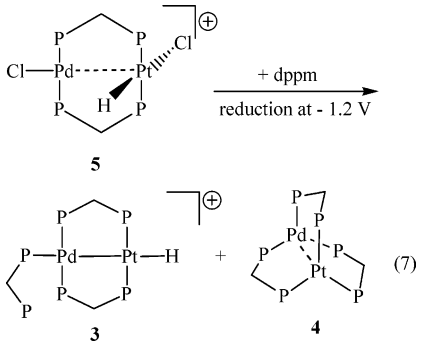

The overall electrochemical reactions for compounds **1**−**5** are summarized in Scheme 3.

Final Comments and Perspectives

There are a lot of similarities between this work and the recent work reported by Krevor and Yee on the electrochemistry of the homodinuclear [$Pt_2(\mu$-dppm$)_2Cl_2$] dimer.[20] The main difference consists of distinct selectivity for the greater lability of the Cl^- ion on the Pt center and the preference for H^- and H^+ to bind to Pt. This study has also shown that the electrochemical investigations offer the opportunity to reliably generate the redox products if they ought to be stable. In this work, the use of some reducing agent proved futile. We are currently exploring the assembly of heterotrinuclear cluster compounds by exploiting the propensity of the pendent dppm ligand of **2a** and **3** to ligate to reactive metal fragments. We are, furthermore, investigating in more detail the parameters that influence the bonding mode of the CNR ligand (bridging vs terminal) in compounds of type **6**, their transformation to bis-isonitrile- and μ-aminocarbyne complexes, and the electrochemistry and photophysics associated with them.

Acknowledgment. P.D.H. thanks NSERC (Natural Sciences and Engineering Research Council) for funding. Y.M. is grateful to the CNRS (Centre National de la Recherche Scientifique) and the Conseil Régional de Bourgogne for funding.

Supporting Information Available: X-ray crystallographic files available for **1**, **2b**, and **6c**, the experimental and simulated ^{31}P NMR spectrum of **2a**, and the ^{1}H NMR spectra of **3** and **5** in the hydride region. This material is available free of charge via the Internet at http://pubs.acs.org.

IC051102Z

(50) Meilleur, D.; Rivard, D.; Harvey, P. D.; Gauthron, I.; Lucas, D.; Mugnier, Y. *Inorg. Chem.* **2000**, *39*, 2909.
(51) *Handbook of Chemistry and Physics*, 64th ed.; CRC Press: Boca Raton, FL, 1983−1984; p D167.
(52) [Pd_2(dppm)$_2Cl_2$] is unreactive toward HPF_6, whereas [Pt_2(dppm)$_2Cl_2$] is reactive. The reduction wave at −1.65 V vs SCE for [Pt_2(dppm)$_2$-Cl_2] is also replaced by two waves at −0.72 and −1.25 V.